

Relativistic mean field study of the properties of $Z=117$ nucleus and the decay chains of $^{293,294}117$ isotopes

M. Bhuyan^{1,2}, S. K. Patra¹ and Raj K. Gupta³

¹ *Institute of Physics, Sachivalaya Marg, Bhubaneswar-751 005, India.*

² *School of Physics, Sambalpur University, Jyotivaha, Sambalpur-768 019, India.*

³ *Department of Physics, Panjab University, Chandigarh-160 014, India.*

(Dated: October 28, 2018)

We have calculated the binding energy, root-mean-square radius and quadrupole deformation parameter for the recently synthesized superheavy element $Z=117$, using the axially deformed relativistic mean field (RMF) model. The calculation is extended to various isotopes of $Z=117$ element, starting from $A=286$ till $A=310$. We predict almost spherical structures in the ground state for almost all the isotopes. A shape transition appears at about $A=292$ from prolate to an oblate shape structures of $Z=117$ nucleus in our mean field approach. The most stable isotope (largest binding energy per nucleon) is found to be the $^{288}117$ nucleus. Also, the Q -value of α -decay Q_α and the half-lives T_α are calculated for the α -decay chains of $^{293}117$ and $^{294}117$, supporting the magic numbers at $N=172$ and/ or 184.

PACS numbers: 21.10.Dr, 21.10.Ft, 21.10.Gv, 21.10.Tg

I. INTRODUCTION

Nuclei can survive beyond the macroscopic limit, far into the transuranium region, where the necessary balance between the nuclear and Coulomb force is achieved only through shell stabilisation. Superheavy element (SHE) are hypothesised to exist in this region. The next double shell closer, beyond ^{208}Pb , predicted at $Z=114$, $N=184$, may have surprisingly long half-life, even of the order of a million year [1–5].

Experimentally, till to-date, elements upto $Z=118$ have been synthesised by heavy ion reactions [6, 7], with half-lives ranging from a few minutes to about a milli-second. The more microscopic theoretical calculations have predicted the next region of stability, beyond $Z=82$, $N=126$, as $Z=120$, $N=172$ or 184 [8–10] and $Z=124$ or 126, $N=184$ [11, 12]. However, the recent experimental possibility of $Z=122$ from natural $^{211,213,217,218}\text{Th}$ -isotopes, associated with long lived superdeformed (SD) and/ or hyperdeformed (HD) isomeric states [13–15], by 16 to 22 orders of magnitude longer than their corresponding ground-state, and more recently the synthesis of $Z=117$ at Flerov Laboratory [16] from the reaction $^{48}\text{Ca}+^{249}\text{Bk}\rightarrow^{297}117$ ($Z=117$, $A=297$), which decay simultaneously via three and four neutrons into two different isotopes $^{293}117$ and $^{294}117$, motivates us to focus on their properties, using a microscopic theoretical model with better predictive power. Such estimations of structure properties of nuclei in the superheavy mass region is a challenging area in nuclear physics and a fruitful path towards the understanding of “Island of stability” beyond the spherically doubly-magic nucleus ^{208}Pb .

The paper is organised as follows. Section II gives a brief description of the relativistic mean field formalism. The pairing effects for open shell nuclei, included in our calculations, are the same as discussed in [15]. The results of our calculation are presented in Section III, and Section IV includes the α -decay modes of $^{293}117$ and $^{294}117$ isotopes. A summary of our results, together with the concluding remarks, are given in the last Section V.

II. THE RELATIVISTIC MEAN-FIELD (RMF) METHOD

The relativistic Lagrangian density for a nucleon-meson many-body system [17, 18],

$$\begin{aligned} \mathcal{L} = & \bar{\psi}_i \{ i\gamma^\mu \partial_\mu - M \} \psi_i + \frac{1}{2} \partial^\mu \sigma \partial_\mu \sigma - \frac{1}{2} m_\sigma^2 \sigma^2 \\ & - \frac{1}{3} g_2 \sigma^3 - \frac{1}{4} g_3 \sigma^4 - g_s \bar{\psi}_i \psi_i \sigma - \frac{1}{4} \Omega^{\mu\nu} \Omega_{\mu\nu} \\ & + \frac{1}{2} m_w^2 V^\mu V_\mu + \frac{1}{4} c_3 (V_\mu V^\mu)^2 - g_w \bar{\psi}_i \gamma^\mu \psi_i V_\mu \\ & - \frac{1}{4} \vec{B}^{\mu\nu} \cdot \vec{B}_{\mu\nu} + \frac{1}{2} m_\rho^2 \vec{R}^\mu \cdot \vec{R}_\mu - g_\rho \bar{\psi}_i \gamma^\mu \vec{\tau} \psi_i \cdot \vec{R}_\mu \\ & - \frac{1}{4} F^{\mu\nu} F_{\mu\nu} - e \bar{\psi}_i \gamma^\mu \frac{(1 - \tau_{3i})}{2} \psi_i A_\mu. \end{aligned} \quad (1)$$

All the quantities have their usual well known meanings. From the above Lagrangian we obtain the field equations for the nucleons and mesons. These equations are solved by expanding the upper and lower components of the Dirac spinors and the boson fields in an axially deformed harmonic oscillator basis, with an initial deformation β_0 . The set of coupled equations is solved numerically by a self-consistent iteration method. The centre-of-mass motion energy correction is estimated by the usual harmonic oscillator formula $E_{c.m.} = \frac{3}{4}(41A^{-1/3})$. The quadrupole deformation parameter β_2 is evaluated from the resulting proton and neutron quadrupole moments, as $Q = Q_n + Q_p = \sqrt{\frac{16\pi}{5}} \left(\frac{3}{4\pi} A R^2 \beta_2 \right)$.

The root mean square (rms) matter radius is defined as $\langle r_m^2 \rangle = \frac{1}{A} \int \rho(r_\perp, z) r^2 d\tau$, where A is the mass number, and $\rho(r_\perp, z)$ is the deformed density. The total binding energy and other observables are also obtained by using the standard relations, given in [18]. We use the well known NL3 parameter set [19]. This set reproduces the properties of not only the stable nuclei but also well predicts for those far from the β -stability valley. As outputs, we obtain different potentials, densities, single-particle energy levels, radii, deformations and the binding energies. For a given nucleus, the maximum binding energy corresponds to the ground state and other solutions are obtained

as various excited intrinsic states.

The constant gap, BCS-pairing approach is reasonably valid for nuclei in the valley of β -stability line. However, this method breaks down when the coupling of the continuum becomes important. In the present study, we deal with nuclei on or near the valley of stability line since the superheavy elements, though very exotic in nature, lie on the β -stability line. In order to take care of the pairing effects in the present study, we use the constant gap for proton and neutron, as given in [20], which are valid for nuclei both on or away from the stability line (for more details, see, e.g., Ref. [15], where E_{pair} , the pairing energy, is also defined).

III. RESULTS AND DISCUSSION

In many of our previous works and of other authors [10, 18, 19, 21–23], the ground state properties, like the binding energies (BE), pairing energies E_{pair} , quadrupole deformation parameters β_2 , charge radii (r_{ch}), and other bulk properties, are evaluated by using the above stated relativistic Lagrangian for different forces. From these predictions, it is found that, generally speaking, most of the recent parameter sets reproduce well the ground state properties, not only of stable normal nuclei but also of exotic nuclei far away from the valley of β -stability. This means to say that if one uses a reasonably well accepted parameter set, the predictions of the model will remain nearly force independent. In this paper we have used the successful NL3 parameter sets for our calculation.

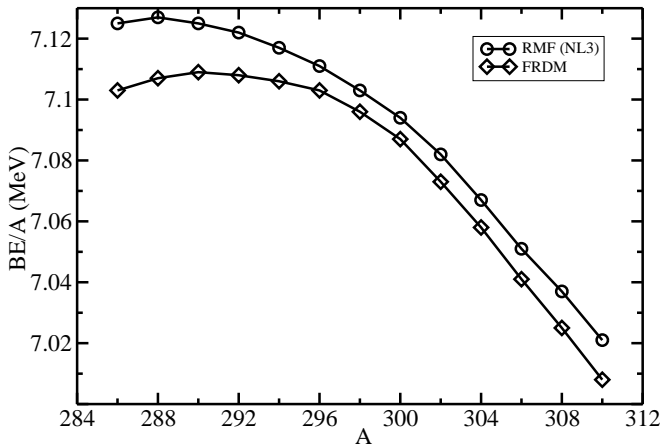


FIG. 1: The binding energy per particle BE/A for the $^{284-310}_{117}$ isotopes, obtained in RMF(NL3) formalism and compared with the FRDM results [24], wherever available.

A. Binding energy and two-neutron separation energy

The calculated binding energy per nucleon BE/A and binding energy BE , obtained from the RMF(NL3) formalism, are

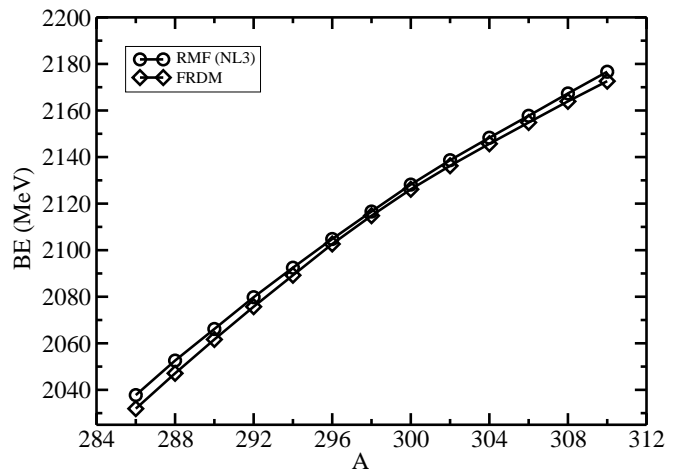


FIG. 2: The total binding energy BE for $^{284-310}_{117}$ nuclei in RMF(NL3) compared with the FRDM results [24].

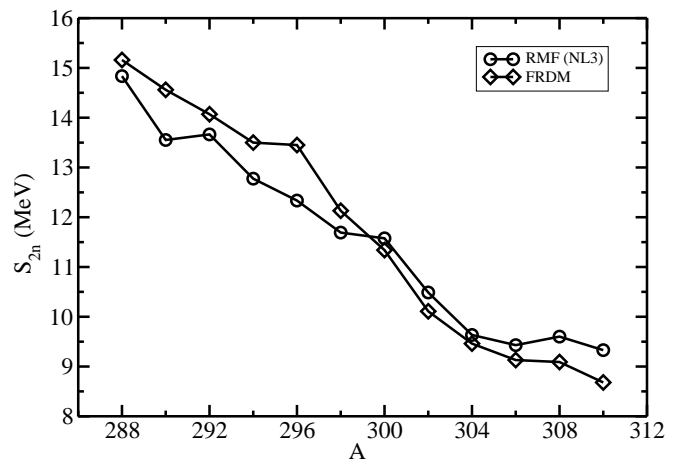


FIG. 3: The two-neutron separation energy S_{2n} for $^{286-310}_{117}$ nuclei, obtained from RMF(NL3) formalisms, and compared with the FRDM results [24], wherever available.

compared, respectively, in Figs. 1 and 2 and in Table I, with the Finite Range Droplet Model (FRDM) results [24]. We notice that the BE/A obtained in the RMF(NL3) model overestimate the FRDM result. In general, the BE/A value starts increasing with the increase of mass number A , reaching a peak value at $A=288$ for RMF(NL3) and at $A=290$ for the FRDM formalism. This means to say that $^{288}_{117}$ is the most stable isotope from the RMF(NL3) result and $^{290}_{117}$ from the FRDM predictions. Interestingly, $^{288}_{117}$ (with $N=171$) and $^{290}_{117}$ (with $N=173$) are both closer to the predicted closed shell at $N=172$ than at $N=184$. Note that the isotopes $^{300,302}_{117}$, next to the magic number $N=184$, are also included in this study. For the total binding energy BE of the isotopic chain in Table I and Fig. 2, we notice that the microscopic RMF binding energies agree well with the macroscopic FRDM calculations, their differences decreasing

TABLE I: The RMF(NL3) results for binding energy BE, two-neutron separation energy S_{2n} , pairing energy E_{pair} , the binding energy difference ΔE between the ground- and first-excited state solutions, and the quadrupole deformation parameter β_2 , compared with the corresponding Finite Range Droplet Model (FRDM) results [24]. The energy is in MeV.

Nucleus	RMF(NL3) Result					FRDM Result		
	BE	S_{2n}	E_{pair}	ΔE	β_2	BE	S_{2n}	β_2
288	2052.586	14.836	14.698	0.333	0.018	2047.09	15.16	0.080
290	2066.138	13.552	14.274	0.360	0.017	2061.65	14.56	0.080
292	2079.802	13.664	14.109	0.096	-0.017	2075.72	14.07	0.072
294	2092.468	12.775	13.653	0.031	0.041	2089.22	13.50	-0.087
296	2104.803	12.335	13.583	0.104	0.028	2102.66	13.45	-0.035
298	2116.598	11.691	13.274	0.389	0.015	2114.79	12.13	-0.008
300	2128.174	11.576	12.841	0.970	0.005	2126.14	11.34	0.000
302	2138.662	10.488	12.623	0.596	0.004	2136.25	10.11	0.000
304	2148.296	9.634	12.695	0.012	0.002	2145.71	9.46	0.000
306	2157.726	9.430	12.348	0.004	0.030	2154.84	9.13	0.000
308	2167.327	9.601	11.912	0.304	0.047	2163.93	9.09	0.001
310	2176.656	9.329	11.538	0.512	0.051	2172.61	8.68	0.000

gradually towards the higher mass region (around $A=298$), and then beyond this mass number the two curves again showing a similar behavior. Note that $^{298}117$ (with $N=181$) is in this case closer to $N=184$.

The two-neutron separation energy $S_{2n}(N,Z) = BE(N,Z) - BE(N-2,Z)$ is also listed in Table I. From the table, we find that the microscopic RMF S_{2n} values also agree well with the macro-microscopic FRDM calculations. This comparison of S_{2n} for RMF with the FRDM result are further shown in Fig. 3, which clearly shows that the two S_{2n} values coincide remarkably well, except at masses $A=290$ and 296 . Apparently, the S_{2n} decrease gradually with increase of neutron number, except for the noticeable kinks at $A=290$ (with $N=173$) and $A=300$ (with $N=183$) in RMF, and at $A=296$ (with $N=179$) in FRDM. Interestingly, these neutron numbers for RMF(NL3) are close to the earlier predicted [8–10] $N=172$ or 184 magic numbers.

B. Shape co-existence

We have also calculated, for the whole $Z=117$ isotopic chain, the solutions in both prolate and oblate deformed configurations. In many cases, we find low lying excited states. As a measure of the energy difference between the ground band-head and the first excited state, we have plotted in Fig. 4 (a) the binding energy difference ΔE between the two solutions, noting that the maximum binding energy solution refers to the ground state (g.s.) and all other solutions to the intrinsic excited state (e.s.). From Fig. 4 (a), we notice that in RMF calculations, the energy difference ΔE is small for the whole region of the considered isotopic series. This small difference in the binding energy for neutron-deficient isotopes is an indication of the presence of shape co-existence. In other words, the two solutions in these nuclei are almost degenerate for a small difference of output in energy. For example, in $^{290}117$, the two solutions for $\beta_2=0.017$ and 0.123 are completely degenerate with the binding energies 2066.138 and 2065.778 MeV. This later result means to suggest that the ground state can be changed to the excited state, and vice-versa, by a small change

in the input data, like the pairing strength, etc., in the calculations. In any case, such a phenomenon is known to exist in many other regions of the periodic table [25].

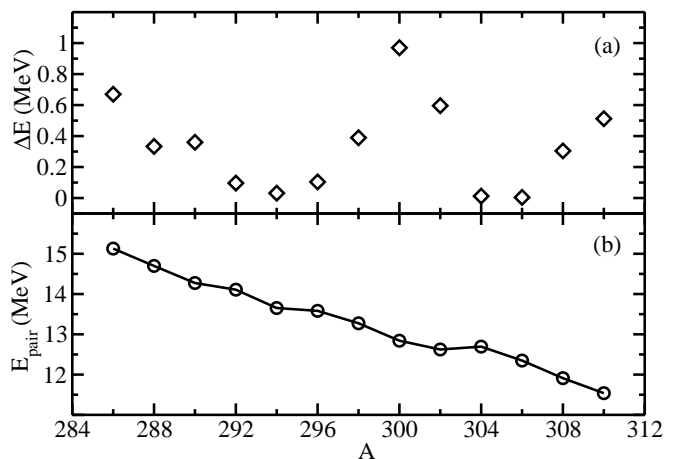


FIG. 4: (a) The energy difference between the ground-state and the first-excited state ΔE , and (b) the pairing energy E_{pair} , for the relativistic RMF(NL3) calculation of $Z=117$ isotopic chain.

Pairing is important for open shell nuclei whose value, for a given nucleus, depends only marginally on quadrupole deformation β_2 . This means that for differing β_2 -values in a nucleus, the pairing energy E_{pair} changes only marginally (by ~ 5 -6%). On the other hand, even if the β_2 values for two nuclei are same, the E_{pair} 's could be different from one another, depending on the filling of the nucleons. This result is illustrated in Fig. 4 (b) for the RMF(NL3) calculation, where E_{pair} for both the g.s. and first-excited state (e.s.), referring to different β_2 -values, are plotted for the full isotopic chain. It is clear from Fig. 4(b) that E_{pair} decreases with increase in mass number A , i.e., even if the β_2 values for two nuclei are the same, the E_{pair} 's are different from one another. This change of E_{pair} is $\sim 15\%$ in going from, say, $A=286$ to 310 .

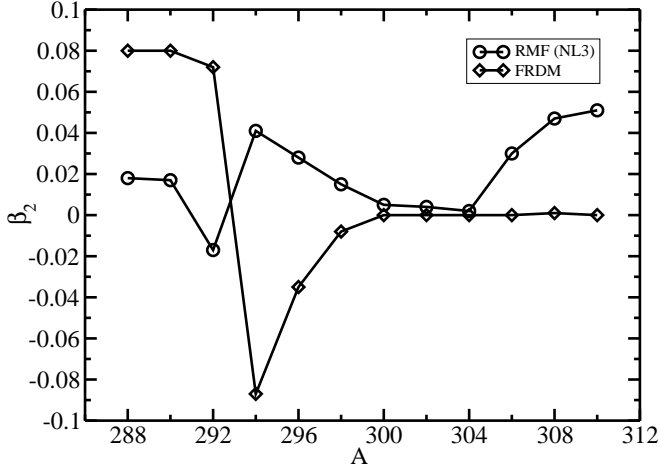


FIG. 5: Quadrupole deformation parameter obtained from relativistic mean field formalism RMF(NL3), Compared with the FRDM results [24], wherever available.

C. Quadrupole deformation parameter

The quadrupole deformation parameter β_2 , for both the ground and first excited states, are also determined within the RMF formalism. In some of the earlier RMF and Skyrme Hartree-Fock (SHF) calculations, it was shown that the quadrupole moment obtained from these theories reproduce the experimental data pretty well [10, 17–19, 21, 26–29]. The g.s. quadrupole deformation parameter β_2 is plotted in Fig. 5 for RMF, and compared with the FRDM results [24]. It is clear from this figure that the FRDM results differ from the RMF(NL3) results for some mass regions. For example, the g.s. oblate solution appear for the nucleus $^{292}117$ in RMF but is a prolate solution in FRDM. A more careful inspection shows that the solutions for the whole isotopic chain are prolate, except at $A=292$ for RMF and at $A=294-298$ for FRDM model. In other word, there is a shape change from prolate to oblate at $A=292$ for RMF and at $A=294$ for FRDM. Interestingly, most of the isotopes are almost spherical in their g.s. configurations.

D. Nuclear radii

The root-mean-square matter radius (r_m) and charge radius (r_{ch}) for the RMF(NL3) formalism are shown in Fig. 6. As expected, the matter distribution radius r_m increases with increase of the neutron number. However, though the proton number $Z=117$ is constant for the isotopic series, the r_{ch} value also increases with neutron number. A detailed inspection of Fig. 6 shows that, in the RMF calculations, both the radii show the monotonic increase of radii till $A=310$, with a jump to a lower value at $A=292$ (with $N=175$). There is no data or other calculation available for comparisons.

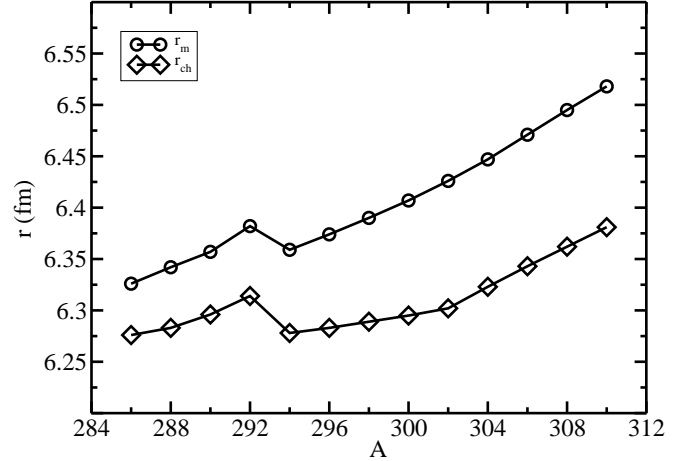


FIG. 6: The rms radii r_m of matter distribution and charge radii r_{ch} for $^{286-310}117$ nuclei, using the relativistic mean field formalism RMF(NL3).

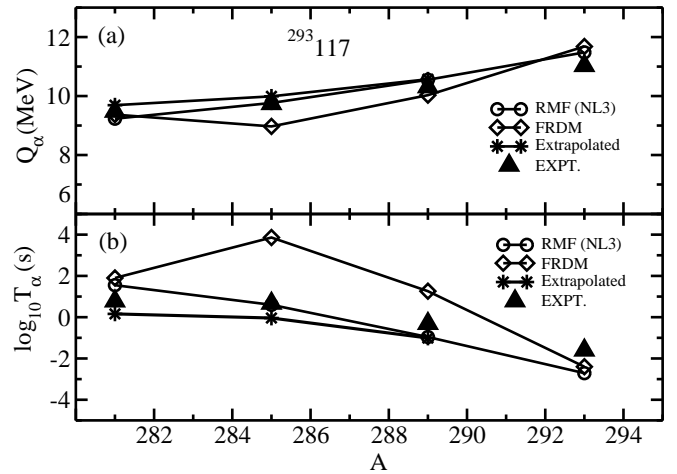


FIG. 7: (a) The Q_α -energy and (b) the half-life time T_α for α -decay series of $^{293}117$ nucleus, using the relativistic mean field formalism RMF(NL3), compared with the FRDM data [24], the extrapolated experimental data [32, 33] and the experimental data [16], wherever available.

IV. THE Q_α ENERGY AND THE DECAY HALF-LIFE T_α

The Q_α energy is obtained from the relation [30]:

$$Q_\alpha(N, Z) = BE(N, Z) - BE(N - 2, Z - 2) - BE(2, 2).$$

Here, $BE(N, Z)$ is the binding energy of the parent nucleus with neutron number N and proton number Z , $BE(2, 2)$ is the binding energy of the α -particle (^4He), i.e., 28.296 MeV, and $BE(N - 2, Z - 2)$ is the binding energy of the daughter nucleus after the emission of an α -particle.

TABLE II: The Q_α energy and T_α for α -decay series of $^{293}117$ nucleus, calculated on the RMF(NL3) model, and compared with the Finite Range Droplet Model (FRDM) results [24], the extrapolated data [32, 33] and the experimental data [16], wherever available. The energy is in MeV and the half-life time in second.

Nucleus	Z	RMF (NL3) Result			FRDM Results			Extrapolated result			Experimental Results	
		BE	Q_α	T_α	BE	Q_α	T_α	BE	Q_α	T_α	Q_α	T_α
293	117	2086.602	11.480	-2.71	2083.06	11.68	-2.40				11.03	-1.60
289	115	2069.786	10.552	-0.96	2066.45	10.03	1.26	2063.17	10.57	-1.01	10.31	-0.31
285	113	2052.042	9.765	0.60	2048.18	8.97	3.86	2045.45	9.99	-0.04	9.74	0.67
281	111	2033.511	9.231	1.55	2028.85	9.37	1.90	2027.13	9.69	0.16	9.48	0.78

TABLE III: Same as for Table II, but for $^{294}117$ nucleus.

Nucleus	Z	RMF (NL3) Result			FRDM Results			Extrapolated result			Experimental Results	
		BE	Q_α	T_α	BE	Q_α	T_α	BE	Q_α	T_α	Q_α	T_α
294	117	2092.578	10.763	-0.906	2089.22	11.66	-3.13				10.81	-1.03
290	115	2075.045	11.083	-2.325	2072.59	9.93	0.77	2069.730	10.329	-0.358	9.95	0.714
286	113	2057.832	9.612	1.055	2054.22	8.90	3.32	2051.764	9.752	0.639	9.63	1.002
282	111	2039.148	9.080	2.027	2034.82	8.80	2.95	2033.220	9.464	0.830	9.00	2.286
278	109	2019.932	8.775	2.316	2015.32	9.38	0.41	2014.388	9.176	1.028	9.55	-0.099
274	107	2000.411	8.105	3.913	1996.40	8.71	1.81	1995.268	8.348	3.042	8.80	1.517

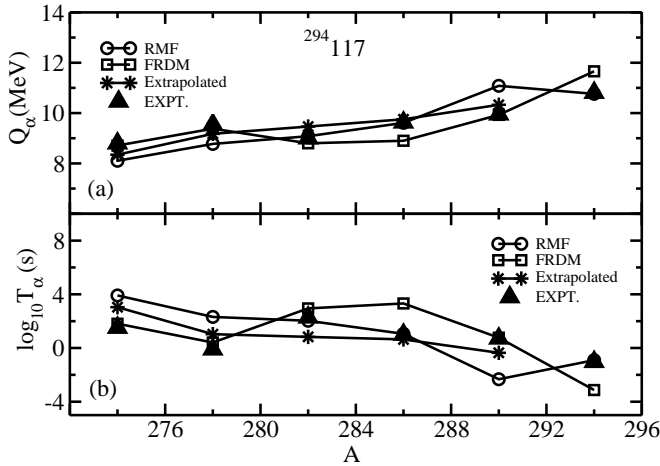


FIG. 8: Same as for Fig. 7, but for $^{294}117$ nucleus.

With Q_α energy at hand, we estimate the half-life $\log_{10}T_\alpha(s)$ by using the phenomenological formula of Viola and Seaborg [31]:

$$\log_{10}T_\alpha(s) = \frac{aZ - b}{\sqrt{Q_\alpha}} - (cZ + d).$$

Here, Z is the atomic number of parent nucleus, and $a=1.66175$, $b=8.5166$, $c=0.20228$ and $d=33.9069$.

A. The α -decay series of $^{293}117$ nucleus

The binding energies of the parent and daughter nuclei are obtained by using the RMF formalism. From these BE, we evaluate the Q_α energy and the half-life time $\log_{10}T_\alpha(s)$, using the above formulae. Our predicted results for the decay chain

of $^{293}117$ are compared in Table II with the finite range droplet model (FRDM) calculation [24], the extrapolated [32, 33] and the experimental data [16], wherever possible. The same comparison is also carried out in Figs. 7 (a) and 7 (b), respectively, for Q_α energy and the half-life time $\log_{10}T_\alpha(s)$.

From Figs. 7(a) and (b), and Table II, we notice that the calculated values for both Q_α and $T_\alpha(s)$ agree well with the known extrapolated as well as experimental data, but are over-estimated with-respect-to the FRDM predictions. For example, the values of T_α from RMF coincide well for the whole mass region with the available experimental data, and with extrapolated values for ^{281}Rg , $^{285}113$ and $^{289}115$ nuclei. Similarly, for ^{281}Rg , the FRDM predictions match both the extrapolated and experimental results. Furthermore, the possible shell structure effects in Q_α , as well as in $T_\alpha(s)$, are noticeable for the daughter nucleus $^{285}113$ (with $N=172$) for both the RMF predictions and experimental data. Note that $N=172$ refers to the predicted magic number.

B. The α -decay series of $^{294}117$ nucleus

In this subsection, we present the Q_α and the $\log_{10}T_\alpha(s)$ results for decay series of $^{294}117$ nucleus, using the same procedure as in the previous subsection for $^{293}117$. The results obtained are listed in Table III and plotted in Figs. 8(a) and 8(b), compared with the FRDM predictions [24], the extrapolated [32, 33] and experimental data [16], wherever possible.

From Fig. 8(a) and (b), and Table III, we found almost similar results as are predicted in the previous subsection for $^{293}117$. Thus, the RMF(NL3) results for both Q_α and $T_\alpha(s)$ agree well with the known extrapolated and experimental data, but once again over-estimate the FRDM results. For example, the T_α values for RMF coincide well with the experimental data for the whole isotopic chain and with the extrapolated data for $^{290}115$, $^{286}113$, ^{282}Rg , ^{278}Mt and ^{274}Bh nuclei. Similarly, FRDM predictions for ^{278}Mt and $^{290}115$ match the ex-

trapolated and for ^{274}Bh and ^{278}Mt with experimental results. The possible shell structure effects in Q_α , as well as in $T_\alpha(s)$, are noticed for the daughter nucleus $^{286}\text{113}$ (with $N=173$) for RMF and ^{278}Mt (with $N=169$) in experimental data, again coinciding with earlier predicted $N=172$ magic number.

V. SUMMARY

Summarizing, we have calculated the binding energy, the rms charge and matter radii, and quadrupole deformation parameter for the isotopic chain of recently synthesized $Z=117$ superheavy element for both the ground- as well as intrinsic first-excited states, using the RMF formalism. From the calculated binding energy, we have also estimated the two-neutron separation energy and the energy difference between ground- and first-excited state for studying the shape co-existence, for the isotopic chain. Also, we have estimated the pairing energy for the ground-state solution in the whole isotopic chain.

We found a shape change from oblate to prolate deformation, with increase of isotopic mass number, at $A=292$. Most of the ground-state structures are with spherical solutions, in agreement with the FRDM calculations. From the binding energy analysis, we found that the most stable isotope in the series is $^{288}\text{117}$, which is close to predicted magic number at $N=172$. Our predicted α -decay energy Q_α and half-life time T_α match nicely with the available extrapolated and experimental data. Some shell structure is also observed in the calculated quantities at $N=172$ and/ or 184 from RMF calculations of the various isotopes of $Z=117$ nucleus.

Acknowledgments

We thanks to Mr. B. B. Pani and Mr. B. K. Sahu for discussion. This work is supported in part by the UGC-DAE Consortium for Scientific Research, Kolkata Center, Kolkata, India (Project No. UGC-DAE CRS/KC/CRS/2009/NP06/1354).

-
- [1] W. D. Myers and W. J. Swiatecki, Report UCRL No. 11980 (1965).
- [2] A. Sobczewski, F. A. Gareev, and B. N. Kalinkin, Phys. Lett. **22**, 500 (1966).
- [3] H. Meldner, in *Proceedings of the International Lysekil Symposium*, Sweden, August 21-27, 1966; Ark. Fys. **36**, 593 (1967).
- [4] U. Mosel and W. Greiner, Z. Phys. **222**, 261 (1969).
- [5] M. Gupta and T. W. Burrow, Nucl. Data Sheets for $A=226-294$, **106**, 251 (2005).
- [6] S. Hofmann and G. Münzenberg, Rev. Mod. Phys. **72**, 733 (2000).
- [7] Yu. Oganessian, J. Phys. G: Nucl. Part. Phys. **34**, R165 (2007).
- [8] K. Rutz, M. Bender, T. Bürvenich, T. Schilling, P. -G. Reinhardt, J. A. Maruhn, and W. Greiner, Phys. Rev. C **56**, 238 (1997).
- [9] R. K. Gupta, S. K. Patra, and W. Greiner, Mod. Phys. Lett. A **12**, 1727 (1997).
- [10] S. K. Patra, C. -L. Wu, C. R. Praharaaj, and R. K. Gupta, Nucl. Phys. A **651**, 117 (1999).
- [11] S. Cwiok, J. Dobaczewski, P. -H. Heenen, P. Magierski, and W. Nazarewicz, Nucl. Phys. A **611**, 211 (1996); S. Cwiok, W. Nazarewicz, and P. H. Heenen, Phys. Rev. Lett. **83**, 1108 (1999).
- [12] A. T. Kruppa, M. Bender, W. Nazarewicz, P. -G. Reinhard, T. Vertse, and S. Cwiok, Phys. Rev. C **61**, 034313 (2000).
- [13] A. Marinov, I. Rodushkin, Y. Kashiv, L. Halicz, I. Segal. A. Pape, R. V. Gentry, H. W. Miller, D. Kolb, and R. Brandt, Phys. Rev. C **76**, 021303(R) (2007).
- [14] A. Marinov, I. Rodushkin, D. Kolb, A. Pape, Y. Kashiv, R. Brandt, R. V. Gentry, and H. W. Miller, arXiv:0804.3869v1 [nucl-ex]; A. Marinov, I. Rodushkin, A. Pape, Y. Kashiv, D. Kolb, R. Brandt, R. V. Gentry, H. W. Miller, L. Halicz, and I. Segal, Int. J. Mod. Phys. E **18**, 621 (2009).
- [15] S. K. Patra, M. Bhuyan, M. S. Mehta and R. K. Gupta, Phys. Rev. C **80**, 034312 (2009).
- [16] Yu. Ts. Oganessian *et al.*, Phys. Rev. Lett. **104**, 142502 (2010).
- [17] B. D. Serot and J. D. Walecka, Adv. Nucl. Phys. **16**, 1 (1986).
- [18] Y. K. Gambhir, P. Ring, and A. Thimet, Ann. Phys. (N.Y.) **198**, 132 (1990).
- [19] G. A. Lalazissis, J. König, and P. Ring, Phys. Rev. C **55**, 540 (1997).
- [20] D. G. Madland and J. R. Nix, Nucl. Phys. A **476**, 1 (1981); P. Möller and J.R. Nix, At. Data and Nucl. Data Tables **39**, 213 (1988).
- [21] P. Arumugam, B. K. Sharma, S. K. Patra, and R. K. Gupta, Phys. Rev. C **71**, 064308 (2005).
- [22] S. K. Patra, R. K. Gupta, B. K. Sharma, P. D. Stevenson, and W. Greiner, J. Phys. G: Nucl. Part. Phys. **34**, 2073 (2007).
- [23] S. K. Patra, F. H. Bhat, R. N. Panda, P. Arumugam, and R. K. Gupta, Phys. Rev. C **79**, 044303 (2009)
- [24] P. Möller, J. R. Nix, W. D. Wyers, and W. J. Swiatecki, At. Data and Nucl. Data Tables **59**, 185 (1995); P. Möller, J. R. Nix, and K. -L. Kratz, At. Data and Nucl. Data Tables **66**, 131 (1997).
- [25] S. Yoshida, S. K. Patra, N. Takigawa, and C. R. Praharaaj, Phys. Rev. C **50**, 1398 (1994); S. K. Patra, S. Yoshida, N. Takigawa, and C. R. Praharaaj, Phys. Rev. C **50**, 1924 (1994); S. K. Patra and C. R. Praharaaj, Phys. Rev. C **47**, 2978 (1993); J. P. Maharana, Y. K. Gambhir, J. A. Sheikh, and P. Ring, Phys. Rev. C **46**, R1163 (1992).
- [26] P. -G. Reinhard and H. Flocard, Nucl. Phys. A **584**, 467 (1995).
- [27] E. Chabanat, P. Bonche, P. Hansel, J. Meyer, and R. Schaeffer, Nucl. Phys. A **627**, 710 (1997).
- [28] E. Chabanat, P. Bonche, P. Hansel, J. Meyer, and R. Schaeffer, Nucl. Phys. A **635**, 231 (1998).
- [29] B. A. Brown, Phys. Rev. C **58**, 220 (1998).
- [30] S. K. Patra and C. R. Praharaaj, J. Phys. G **23**, 939 (1997).
- [31] V. E. Viola, Jr. and G. T. Seaborg, J. Inorg. Nucl. Chem. **28**, 741 (1966).
- [32] Yu. Ts. Oganessian *et al.*, Phys. Rev. C **72**, 034611 (2005).
- [33] G. Audi, A. H. Wapstra, and C. Thibault, Nucl. Phys. A **729**, 337 (2003).